Journal of Soils and Sediments (2022) 22:238–255
https://doi.org/10.1007/s11368-021-03070-2

SOILS, SEC 5 • SOIL AND LANDSCAPE ECOLOGY • RESEARCH ARTICLE

Prediction of dimensionless sediment transport capacity for loess slopes and its response to flow intensity parameters

Jingwen Wang[1] · Chenye Gao[2,3] · Xile Liu[3] · Guangming Tan[1]

Received: 17 May 2021 / Accepted: 3 September 2021 / Published online: 24 September 2021

Abstract

Purpose The sediment transport capacity provides a theoretical basis for accurate prediction of soil erosion. The aim of this study is to develop a sediment transport capacity prediction model applicable to a variety of soils.

Materials and methods Sandy loess and loess soil (d_{50} = 0.095 mm and d_{50}' = 0.04 mm) were used to conduct indoor sediment transport experiments under different hydraulic conditions. Moreover, the experimental data of cohesive soil and cohesionless sand was combined, and the response relationship between sediment transport capacity and each flow intensity parameter was analyzed through dimensionless processing.

Results and discussion Results showed that the sediment transport capacity had an exponential function relationship with unit discharges and energy slopes. The sediment transport capacity also varied with the changing flow intensity parameters, and through analysis, the effective stream power was observed as an optimum predictor (R^2 = 0.9692). Considering the effective stream power and volumetric sediment concentration, this study derived a formula for calculating the sediment transport capacity.

Conclusions In conclusion, this study innovatively established a prediction model of sediment transport capacity on loessial slopes though regression analysis and dimensionless method. The proposed model is capable of considering flow intensities and volumetric sediment concentration simultaneously, and has a superior applicability to both cohesive soil and cohesionless sand compared with the four main existing models.

Keywords Overland flow · Sediment transport capacity · Flow intensity parameters · Effective stream power · Volumetric sediment concentration

1 Introduction

Soil erosion, a major environmental problem, has attracted significant attention worldwide (Ali et al. 2012). The Loess Plateau has significant importance in energy and food production, as well as economic progress. However, severe soil erosion in this area has posed various threats to the environmental sustainability (Liu et al. 2012; Zhao et al. 2013a). More than 70% of the area now is gully-hill-dominated due to intense soil erosion over thousands of years (Tian et al. 2016). Various strategies including continuous soil and water conservation practices have been implemented to mitigate this phenomenon (Zhao et al. 2013b). However, analyzing the water erosion process is still necessary to provide a reference for establishing soil erosion prediction models in sediment transport capacity research.

Water erosion is the most prominent way, which refers to the destruction of soil framework and transportation of particles due to a flowing water. Water erosion consists of three dynamic processes: soil detachment, sediment transport, and sediment deposition. The sediment transport capacity of overland flow mainly represents the maximum flux of sediment transport under specific hydraulic conditions (Huang

Responsible editor: Lu Zhang

✉ Chenye Gao
gaochenye5023@126.com

[1] State Key Laboratory of Water Resources and Hydropower Engineering Science, Wuhan University, Hubei 430072, China

[2] Hangzhou Regional Center(Asia-Pacific) for Small Hydro Power, National Research Institute for Rural Electrification, Hangzhou 310012, China

[3] State Key Laboratory of Soil Erosion and Dryland Farming On the Loess Plateau, Northwest A&F University, Yangling 712100, China

et al. 1999; Li and Abrahams 1999; Zhang et al. 2009). This plays a critical role in determining the areas of net erosion, where the actual sediment concentration is less than the transport capacity, and net deposition, where the transport capacity is exceeded (Yu et al. 2015). This is because of the relationship between sediment concentration and sediment transport capacity (Merten et al. 2001; Nearing et al. 1989). When sediment transport rate is less than sediment transport capacity, the soil detachment dominates; when the rate is equal to the capacity, the detachment and sediment deposition processes could reach a dynamic equilibrium. Adversely, the sediment deposition would occur owing to excessive soil particles transported by currents (Ahmadi et al. 2006). Therefore, accurate prediction of the sediment transport capacity is crucial while investigating soil erosion.

Several factors including energy slopes, slope length, flow discharge, and flow velocity affect the sediment transport capacity of overland flow (Hao et al. 2019; Zhao et al. 2020; Wang et al. 2020a; Li et al. 2020; Wu et al. 2021), and the flow intensity parameters (Liu et al. 2014). These factors can be classified into three categories like slope form, hydraulic parameters, and soil properties (Prosser and Rustomji 2000). The actual slope length in the Loess Plateau area is generally more than tens of meters. However, the test length could not reach that value owing to restricted experimental conditions (Zhang 2000). Zhang et al. (2017) studied relationships between hydraulic parameters and sediment yield under different slope lengths, and concluded that the step length of the fluctuation process in overland flow was three meters. It is noteworthy that relevant studies mainly focused on the relationship between sediment transport capacity and slope gradient, flow discharge, and mean flow velocity (Li et al. 2021; Wang et al. 2020b; Abrahams et al. 2015; Govers et al. 2010; Nearing et al. 1997). For example, Li et al. (2021) proposed that among various flow intensity parameters, the mean flow velocity was significantly correlated with sediment transport capacity ($R^2 = 0.92$). Wang et al (2020b) reported that the slope gradient could modify the soil detachment mechanisms and sediment transport process. Moreover, the sediment transport capacity was closely related to the sediment properties, such as median particle size, liquid viscosity, and shapes of sediment particles (Pieri et al. 2009). With an increasing particle diameter, the incipient settling velocities of soil particles increased exponentially (Zhang et al. 2011), while the sediment transport capacity showed an exponential decline (Govers 1990). Therefore, different hydraulic parameters should be considered while calculating the sediment transport capacity (Wang et al. 2021a, b).

The sediment transport capacity can be calculated using compound hydraulic parameters including shear stress, stream power, and unit stream power (Wu et al. 2018). Finkner et al. (1989) used the flow shear stress τ in Water Erosion Prediction Project model (WEPP), while Beasley et al. (1980) and De Roo (1996) selected the unit stream power P in EUROSEM and LISEM models. However, Mahmoodabadi et al. (2014a, 2014b) reported that sediment transport capacity results obtained through the GUEST model had a higher accuracy than those of the WEPP model. At present, several formulation exists for calculating the sediment transport capacity based on sediment transport theories in open-channels and natural rivers.

Beasley et al. (1980) proposed the formula for sediment transport capacity on the basis of a single influencing factor, as shown in formula (1). It has been applied to the ANSWERS model (Areal Nonpoint Source Watershed Environment Response Simulation).

$$T_c = 146Sq^{0.5}q \le 0.046$$

$$T_c = 14600Sq^2q \ge 0.046 \quad (1)$$

where T_c is the flow sediment transport capacity, $kg{\cdot}m^{-1}{\cdot}s^{-1}$, and S is the energy slope, %. The q is unit discharge, m^2/min.

Finkner et al. (1989) proposed a compound factor and then established the WEPP model (Water Erosion Prediction Project) after simplifying the Yalin formula (Yalin 1963):

$$T_c = K\tau^{3/2} \quad (2)$$

where τ is the shear stress, Pa. The sediment transport coefficient K is a comprehensive coefficient representing the general state of water flows and soil sediments.

Then, Zhang et al. (2008) carried out steep slope tests and found that the sediment transport coefficient K increased in terms of its power function with an increasing shear stress τ. It is also found that the WEPP model underestimated the influence of flow shear stress. So, the WEPP model was revised by considering the exponent as two:

$$T_c = K\tau^2 \quad (3)$$

Ali et al. (2012) obtained the relations between the total flow discharges, median particle size, and energy slope through sediment transport experiments with four different median particle sizes as follows:

$$T_c = 0.17 \times 10^6 \frac{Q^{1.46}}{d_{50}^{0.5}} S^{2.89} \quad (4)$$

where Q is the total flow discharge, m^3/s. d_{50} means the median particle size, mm, and S is the energy slope, %.

Zhang et al. (2011) established a formula for sediment transport capacity which is applicable to sediments with diverse soil characteristics:

$$T_c = 0.024 \sum_{i=1}^{n} d_{50i}^{-0.313} P_i \tau^2 \quad (5)$$

where n is the number of different sediment particle sizes. And d_{50i} represents a particular sediment median particle size, mm. P_i indicates the proportion of a certain median particle size in total sediments.

Furthermore, Luan et al. (2016) simulated the transport process of cohesionless sand on steep slopes and evaluated the influence of stream power on sediment transport capacity. Then, a formula was obtained by analyzing its relation with d_{50i}, P_i, and W:

$$T_c = 0.142 \sum_{i=1}^{n} d_{50i}^{-0.322} P_i W^{1.25} \quad (6)$$

where W is the stream power, $w/\ m^2$.

Apparently, there were no consistent conclusions regarding the selection of flow intensity parameters, and existing prediction models were aimed at a certain kind of soils like cohesive soil and sand, so the prediction model cannot be applied to each other. The novelty of this manuscript is reflected in three aspects: First, as different soil types with diverse median particle size were considered; here, the dimensionless method was adopted to eliminate its influence on flow intensity parameters. Second, this research indicated that the volumetric sediment concentration is a prominent parameter when predicting the sediment transport capacity as it is closely related to the sediment transport coefficient K. Above all, the response relationship between flow intensity parameters and sediment transport capacity was thoroughly analyzed by considering the difference between suspended load and traction load. At last, a formula suitable for cohesive and cohesionless soils was obtained through the implicit function analysis method. The experiment conducted in this study was similar to those of Zhang et al. (2011), Wu et al. (2016), Ail et al. (2012), and Aziz and Scott (1989): these are generally known as sheet flow sediment transport experiments. These experiments only differed in terms of slope gradient, flow discharge, and the median diameter. Therefore, this study synthesized the data of the aforementioned four studies. The objectives of this study were the following:

(1) to evaluate a relationship between dimensionless sediment transport capacity and dimensionless flow intensity parameters.

(2) to establish the sediment transport capacity for sheet flow considering the volumetric sediment concentration and an optimum flow intensity parameter.

(3) to evaluate the applicability of the proposed prediction model by comparing the results with those of the four existing models.

2 Materials and methods

2.1 Soil samples

The test soil materials were Shenmu sand loess from Shenmu county (110°30′E, 38°49′48″N) and Huangmian soil collected from Ansai County (109°19′23″E, 36°51′30″N), as shown in Fig. 1. Table 1 shows the particle size distribution of Shenmu sand loess (d_{50} = 0.095 mm) and Huangmian soil (d_{50} = 0.04 mm).

2.2 Experimental setup

The experimental set-up consisted of a test flume, a constant water tank, a sediment hopper, and sediment collection devices as shown in Fig. 2. An adjustable flume of size 4.5 × 0.3 × 0.1 m^3 (L × W × H) with plexiglass sides was selected in this experiment. The flow discharge was

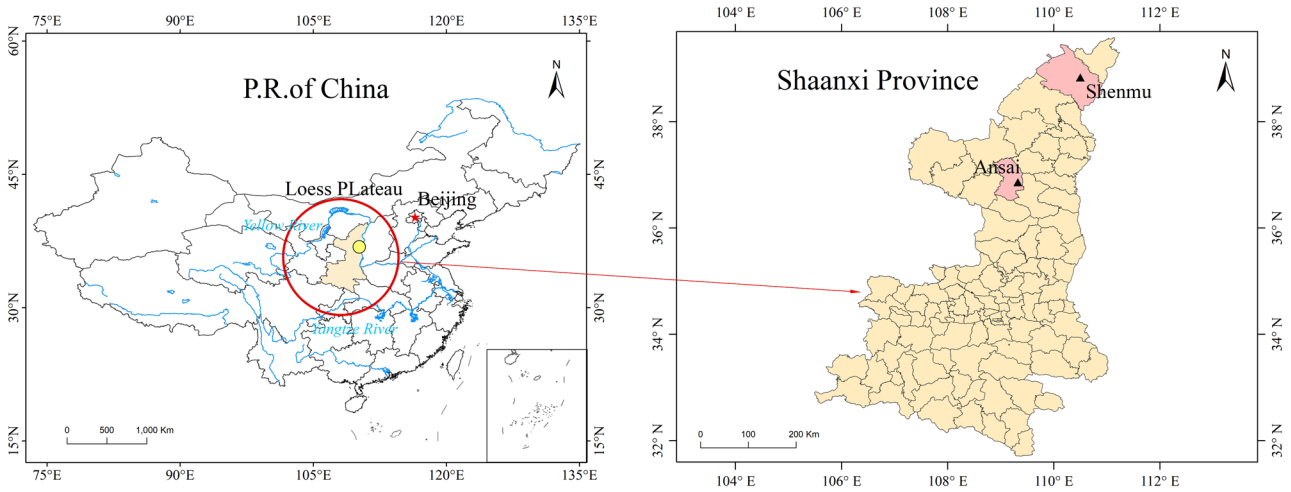

Fig. 1 Location of this test area

Table 1 Particle size distribution of different soil materials

Particle size/mm	Coarse sand > 0.25	Fine sand 0.25 ~ 0.05	Coarse silt 0.05 ~ 0.01	Medium silt 0.01 ~ 0.005	Fine silt 0.005 ~ 0.001	Clay particles < 0.001
d_{50} = 0.095 mm	0.30%	64.9%	22.0%	2.8%	3.2%	5.8%
d_{50} = 0.04 mm	0%	36.58%	48%	3.84%	4.73%	6.85%

controlled by seven drain valves at the outlet of the constant water tank. A sediment hopper which was 0.5 m distant from the upper side of this flume was used to provide the water flow with sediments. The rate of adding sediments was controlled by guide plates and rollers, as shown in Fig. 2. Three slopes (10.5%, 15.6%, and 20.8%) and seven unit discharges (0.27, 0.54, 0.81, 0.108, 0.135, 0.162, and 1.89×10^{-3} m^2 s^{-1}) were systematically investigated using Shenmu sand loessial samples. As for Huangmian soil materials, five types of slopes (7.0%, 10.5%, 14.1%, 17.6%, and 21.3%) and six unit discharges (0.19, 0.39, 0.58, 0.75, 0.95, and 1.12×10^{-3} m^2 s^{-1}) were set up in this test.

2.3 Measurements

Before adding sediments into the water flow, the slope gradient and flow discharges were adjusted to the designed values. Flow discharges were measured by the weighing method with an accuracy of 0.001L/s. After reaching a constant value, related hydraulic parameters were measured. Three cross sections positioned at 1.0, 2.0, and 3.0 m along the slope from top to bottom were observed in this flume. Three measuring points were set on each cross section, and the surface velocity was observed by the KMnO4 dye tracer method (Shang et al. 2020). For surface flow velocity, an average of 20 observations for each point was considered to increase the reliability of the data. Therefore, at each cross section, three relatively accurate surface flow velocities were obtained from the left and right of the flume, as shown in Fig. 3b. A camera was employed to determine the time when the tracer crossed a marked distance (1 m). It is remarkable that the starting and stopping of the time depend on the front of the dyeing currents. Compared with "volumetric flow rate" method, the

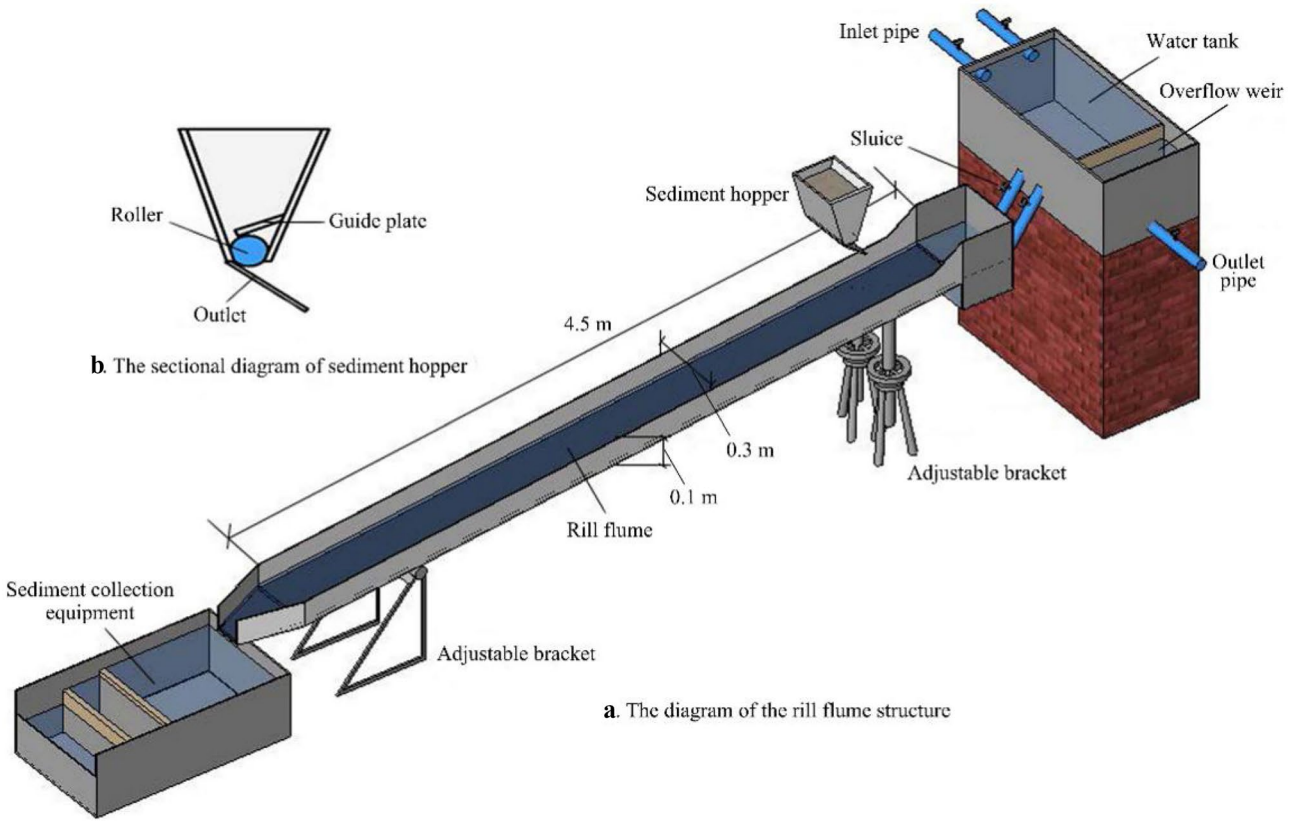

Fig. 2 Schematic of the experimental set-up

(a) Water depth measurement **(b)** Flow velocity measurement

Fig. 3 The measuring method. (**a**) Water depth measurement. (**b**) Flow velocity measurement

centroid velocity of stained spots could better represent the flow velocity because it does not require selection of empirical coefficients and regular flow cross-sections. In addition, compared with salt tracing and electrolytic pulse methods, this KMnO4 dye tracer method would not be affected by sediment concentration and water depth on the slope. The water depth was measured using the SX401 digital probe tester with an accuracy of 0.01 mm, as shown in Fig. 3a. In addition, as shown in Tables 2 and 3, initially, the water depth was shallow and then increased as the flow discharges increased. The sediment transport capacity of loess sand (d_{50} = 0.095 mm) increased comparatively

Table 2 The experimental data (Shenmu sand loess, median particle size = 0.095 mm)

Median particle size/mm	Slope/%	Unit discharge/ $m^2\ s^{-1}$	Water depth/m	Sediment transport capacity/kg $m^{-1}\ s^{-1}$	Mean flow velocity/ $m{\cdot}s^{-1}$
0.095	10.5	0.00029	0.00186	0.0090	0.158
		0.00056	0.00249	0.0350	0.226
		0.00069	0.00304	0.1250	0.226
		0.00093	0.00351	0.1790	0.266
		0.00106	0.00397	0.2870	0.267
		0.00120	0.00433	0.4050	0.277
		0.00162	0.00527	0.7800	0.307
	15.6	0.00028	0.00176	0.0368	0.160
		0.00067	0.00257	0.0778	0.259
		0.00078	0.00300	0.1600	0.259
		0.00086	0.00346	0.2220	0.249
		0.00111	0.00407	0.4100	0.273
		0.00125	0.00450	0.6160	0.278
		0.00153	0.00487	0.9170	0.315
	20.8	0.00031	0.00181	0.0720	0.169
		0.00052	0.00249	0.0820	0.208
		0.00094	0.00313	0.2490	0.300
		0.00115	0.00368	0.3310	0.313
		0.00129	0.00393	0.5470	0.329
		0.00154	0.00443	0.7630	0.347
		0.00188	0.00502	1.0270	0.374

Table 3 The experimental data (Huangmian soil, median particle size = 0.004 mm)

Median particle size/mm	Slope/%	Unit discharge/ $m^2\ s^{-1}$	Water depth/m	Sediment transport capacity/kg $m^{-1}\ s^{-1}$	Mean flow velocity/ $m{\cdot}s^{-1}$
0.04	7.0	0.00039	0.00312	0.0157	0.125
		0.00058	0.00413	0.0282	0.140
		0.00075	0.00322	0.1015	0.233
		0.00095	0.00421	0.1391	0.226
		0.00112	0.00419	0.2052	0.267
	10.5	0.00019	0.00225	0.0088	0.084
		0.00039	0.00231	0.0195	0.169
		0.00058	0.00294	0.0948	0.197
		0.00075	0.00286	0.1634	0.262
		0.00095	0.00313	0.2171	0.304
		0.00112	0.00425	0.3167	0.264
	14.1	0.00019	0.00216	0.0095	0.088
		0.00039	0.00211	0.0532	0.185
		0.00058	0.00336	0.0875	0.173
		0.00075	0.00322	0.1447	0.233
		0.00095	0.00311	0.2102	0.305
		0.00112	0.00396	0.3366	0.283
	17.6	0.00019	0.00314	0.0340	0.061
		0.00039	0.00325	0.0916	0.120
		0.00058	0.00335	0.1700	0.173
		0.00075	0.00312	0.2039	0.240
		0.00095	0.00323	0.2909	0.294
		0.00112	0.00422	0.5242	0.265
	21.3	0.00019	0.00314	0.0660	0.061
		0.00039	0.00243	0.1381	0.160
		0.00058	0.00322	0.1958	0.180
		0.00075	0.00321	0.2889	0.234
		0.00095	0.00334	0.4203	0.284
		0.00112	0.00312	0.5137	0.359

faster as flow discharges and slope gradient increased. Furthermore, when the energy slope and unit discharges were small, the sediment transport capacity of loess sand ($d_{50} = 0.095$ mm) and Huangmian soil ($d_{50} = 0.04$ mm) exhibited some fluctuations. This could be because of the destabilization of sediment-laden flow that generated a series of waves; the wave crests and troughs significantly influenced the observational result when the energy slope and unit discharges were relatively small, as shown in Fig. 4. The appearance and disappearance of roll waves can influence the hydraulics and hydrodynamic force distribution of water flow and therefore influence the sediment transport process (Want et al. 2021). Further, during the process of roll wave propagation, liquid particles on the surface and at the bottom are mixed with each other, resulting in high turbulence intensity (Wang et al. 2019). Thus, the dynamic conditions of sediment incipience and subsidence could be affected by roll waves. Because the sediment concentration at wave crests and troughs was over-saturated and nearly saturated respectively, the number of wave crests and troughs would influence the measurement of sediment concentration in flow-water during the sampling of sediments at the outlet of the flume.

2.4 Experimental procedures

Equation (7) proposed by Zhang et al. (2011) was used to predict an approximate T_c value in advance. It is because these experimental conditions are similar, and they are all indoor simulated tests. Then, numerous pre-experiments with initial sediment discharges approximating this value were carried out. When the sediments in flows just began to settle on the surface of this flume, it was considered that

(a). Wave-current coupling in sediment-laden flow

(b). Wave crest and trough in wave-current coupling

(c). Regular sediment transport in sediment-laden flow

Fig. 4 The sediment transport phenomenon in sediment-laden flow. (**a**) Wave-current coupling in sediment-laden flow. (**b**) Wave crest and trough in wave-current coupling. (**c**) Regular sediment transport in sediment-laden flow

the T_c value at this instant was close to sediment transport capacity, and then the main experiments started.

$$T_c = 2382.32q^{1.269}S^{1.637}d_{50}^{-0.345} \tag{7}$$

where T_c is the sediment transportation capacity of overland flow, kg/(s m), and q is the unit discharge, m^2/s. S means the energy slope, %, and d_{50} is the median particle size, mm.

During the main experiments, each time the flow velocity and water depth were measured, the sediment transport process continued until the flow was unable to transport the sediments. Once the water flow reached the transport capacity, the deposition could be observed on the bed surface (Mu et al. 2019). When measuring the sediment transport capacity, the rate of adding sand was controlled through the electric motor and sediment hopper until it stabilized within five minutes. Moreover, the sediments and water were fully mixed with iron bars. As the discharge of sediment-laden water was constant, sampling buckets with different numbers were used at the outlet of the flume. The sampling time determined by flow discharges and the size of containers were recorded by a stopwatch. After approximately 30 s, the sediment samples were sent to be deposited and dried, and the M value in formula (8) was the average the mass of these sand samples. The sediment transport capacity could be expressed as follows::

$$T_c = \frac{M}{Tb} \tag{8}$$

where M is the mass of dried sand samples, kg. The parameter b is the width of this test flume, while T is the sampling time, s.

2.5 Calculation of hydraulic parameters

In sediment transport mechanics, flow intensity parameters are generally classified into three categories: flow velocity parameters (surface velocity, bottom velocity, and mean velocity), dynamic parameters (flow shear stress), and power parameters (unit stream power, stream power, and effective stream power).

However, owing to discrepancies in the definition of surface velocity and bottom velocity, these two parameters have been rarely used. In the present study, the surface velocity of flow was observed using the $KMnO_4$ dye tracer method to provide a reference to obtain the appropriate mean velocity V. Previous studies have proposed that mean velocity can be estimated by multiplying the surface velocity with a correction coefficient defined as (the ratio of the average to maximum velocity). For example, Luk and Merz (1992), Dunkerley (2010), and Ali et al. (2012) all gave a reasonable correction coefficient. However, in order to avoid some interferences of these correction coefficients, the mean velocity V which has been more extensively used could be expressed as follows:

$$V = \frac{Q}{bh} \tag{9}$$

where V is the mean velocity, m/s, and h is the water depth, m, and b is the width of the flume, m.

The flow shear stress refers to the force acting along slopes during the movement of fluids. It can be expressed as

$$\tau = \rho ghS \tag{10}$$

Table 4 The range of different hydraulic parameters

comparable objects	Median particle size/mm	Slope/%	Unit discharge/m^2 s^{-1}	Mean flow velocity/m s^{-1}	Water depth/mm	Sediment transport capacity/kg m^{-1} s^{-1}
This study	0.095	10.5 ~ 20.8	0.00014 ~ 0.00111	0.158 ~ 0.374	1.86 ~ 5.02	0.009 ~ 1.027
	0.04	7 ~ 20.8	0.00019 ~ 0.00112	0.527 ~ 1.11	1.42 ~ 4.13	0.0088 ~ 0.5243
Wang et al. (2019)	0.04	10.5 ~ 38.4	0.00082 ~ 0.00319	0.474 ~ 1.063	1.08 ~ 3.65	0.1673 ~ 3.4281
Zhang et al (2011)	0.1 ~ 1.16	8.7 ~ 42.3	0.00066 ~ 0.00526	0.218 ~ 0.952	1.98 ~ 8.43	0.07 ~ 8.66
Ali et al. (2012)	0.23 ~ 1.02	5.2 ~ 17.6	0.00007 ~ 0.00207	0.163 ~ 0.473	0.75 ~ 5.65	0.0008 ~ 0.1337
Aziz and Scott (1989)	0.29 ~ 1.02	3 ~ 10	0.00165 ~ 0.00473	0.27 ~ 0.706	3.51 ~ 11.58	0.0089 ~ 0.353

where τ is the flow shear stress, Pa, and ρ is the density of water flow, kg^3/m. g is the acceleration due to gravity (9.81 m/s^2), and the h is water depth, m.

Bagnold (1966) proposed a concept stream power and expressed it as

$$W = \tau V = \rho g S q \tag{11}$$

where W is the stream power, w/m^2. Compared with stream power, the unit stream power considers the mass of water flow. It represents the energy loss of sediment transport per unit mass of water flow.

The relationship between unit stream power and mean velocity, as well as slopes is

$$P = VS \tag{12}$$

where P is the unit stream power, m/s.

Govers (1992) proposed the effective stream power on the basis of flow shear stress, which represents the actual output power of water flows. The formula is

$$W_{\text{eff}} = \frac{(\tau V)^{1.5}}{h^{0.67}} \tag{13}$$

where W_{eff} is the effective stream power, $N^{1.5}/(s^{1.5}\ m^{2.17})$.

2.6 Theoretical analysis

In this study, the experimental data were selected to ensure consistency with Zhang et al. (2011), Wu et al. (2016), Ali et al. (2012), and Aziz and Scott (1989). In total, 348 groups of data were selected as per the availability of data, as shown in Table 4. This is because the aforementioned studies are all flume experiments and there are only differences between the energy slope, flow discharge, and median particle size of soils. In this study, 5.8% and 6.85% cohesive soil particles possessed a median particle size of 0.095 mm and 0.04 mm, respectively; this was consistent with that in Wu et al. (2016). For cohesionless fine, data was selected in conformity with Zhang et al. (2011), Ali et al. (2012), and Aziz and Scott (1989). The parameter was made dimensionless, given the diverse median particle sizes used in different studies, as shown in Table 5. This process considered the settling velocity because in quiescent water, the median particle size has insignificant influence on the sediment settling velocity. When the related flow intensity parameters and the sediment transport capacity are all dimensionless, the influence of median particle size on flow intensity parameters would be weakened.

Table 5 Non-dimensional formulas of flow intensity parameters

Flow intensity parameters	Formulas of flow intensity parameters	Non-dimensional formulas of flow intensity parameters
Mean velocity	V	$V^* = V/\left[\sqrt{\gamma_S/\gamma - 1 g d_{50}}\right]$
Flow stress force	$\tau = \rho g h S$	$\theta = \gamma h J/\left[\left(\gamma_s/\gamma\right) d_{50}\right]$
Unit stream power	$P = VS$	$P * = VS/\omega$
Stream power	$W = \tau V$	$W^* = \theta V^*$
Effective stream power	$W_{eff} = W^{1.5}/h^{0.67}$	$W^*_{eff} = W^{*1.5}/(h/d_{50})^{0.67}$
Sediment transport capacity	$T_c = M/(Tb)$	$\Phi = T_c/\left[\gamma_s\sqrt{(\gamma_s/\gamma - 1 g d_{50}^3}\right]$

γ_s is particle density of sediment particles. γ_s was 2650 (kg/m^3) in this study.γ is water particle density. ω is the settling velocity of sediment particles. J is the energy slope. d_{50} is the median particle size of sediment particles. V^* is the dimensionless mean velocity. θ is the dimensionless shear stress. W^* is the dimensionless stream power. P^* is the dimensionless unit stream power. $W_{\text{eff}}{}^*$ is the dimensionless effective stream power. Φ is the dimensionless sediment transport capacity

Then all data were randomly divided into two groups without human interference. The first group contains 181 sets of data, which could be used to analyze the relationship between flow intensity parameters and sediment transport capacity, and to derive formulas for calculating the sediment transport capacity of overland flow. Another 166 sets of data were chosen to evaluate the applicability of these formulas. When evaluating its applicability, the correlation coefficient R^2 and Nash coefficient N_{SE} were selected to verify the simulation of these formulas (Wu et al. 2021).

$$R^2 = \frac{\left[\sum_{i=1}^{n}\left(O_i-\overline{O}\right)\left(P_i-\overline{P}\right)\right]^2}{\sum_{i=1}^{n}\left(O_i-\overline{O}\right)\sum_{i=1}^{n}\left(P_i-\overline{P}\right)^2} \tag{14}$$

$$N_{SE} = 1-\frac{\sum\left(O_i-P_i\right)^2}{\sum\left(O_i-\overline{O}\right)^2} \tag{15}$$

where P_i is the simulated value and is the average of simulated values. O_i is the measured value, while is the average of measured values.

3 Results and analysis

3.1 Selection of parameters

The response relationship between dimensionless mean velocity V^* and dimensionless sediment transport capacity Φ was shown in Fig. 5a. It showed that the sediment transport capacity Φ increased in terms of its power function with an increasing mean velocity (R^2=0.664). The relation can be expressed by formula (16):

$$\Phi = 0.0214V^{*3.009}R^2 = 0.664 \tag{16}$$

where Φ is the dimensionless sediment transport capacity in overland flow, while V^* is the dimensionless mean velocity. Then, formula (16) was validated by the second set of data, as shown in Fig. 5b. The fitting precision R^2 was 0.957, and the N_{SE} value was 0.664. This formula could better predict the sediment transport capacity of silty sand containing cohesive particles in this test and that of Wu et al. (2016). But it is not suitable for cohesionless sand tests in Zhang et al. (2011), Ali et al. (2012), and Aziz and Scott (1989). Overall, the prediction results using the predictor mean velocity are not that ideal.

The response relationship between dimensionless flow shear stress θ and dimensionless sediment transport capacity Φ was shown in Fig. 6a. It showed that the sediment transport capacity Φ increased in terms of its power function with an increasing flow shear stress (R^2=0.9498). The relation can be expressed by formula (17):

$$\Phi = 0.0369\theta^{2.0307}R^2 = 0.9498 \tag{17}$$

where θ is the dimensionless flow shear stress. Then, formula (17) was validated by the second set of data, as shown in Fig.6b. The fitting precision R^2 was 0.920, and the N_{SE} value was 0.806.

(3) The response relationship between dimensionless stream power W^* and dimensionless sediment trans-

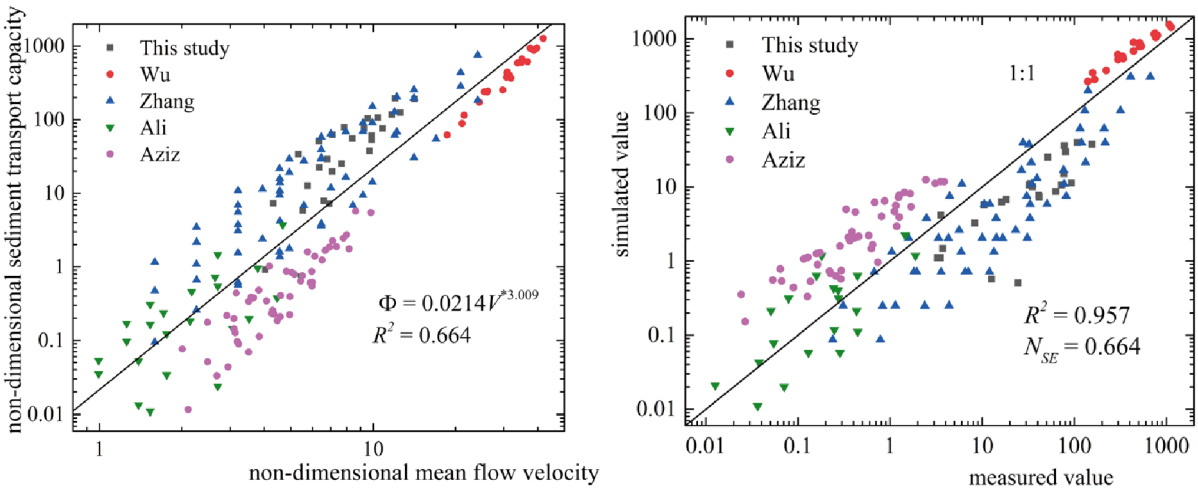

(a). The relationship between Φ and V* **(b).** The comparision of simulated and measured values in formula (16)

Fig. 5 Relationships between Φ and *V** and the fitting precision of formula (16). (**a**) The relationship between Φ and *V**. (**b**) The comparison of simulated and measured values in formula (16)

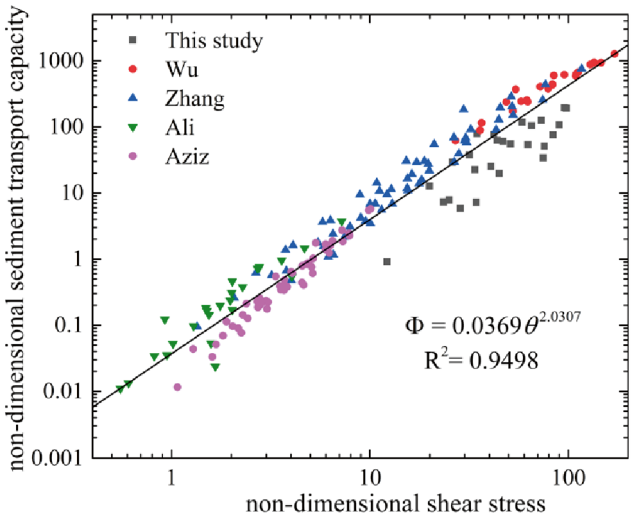

(a). The relationship between Φ and θ

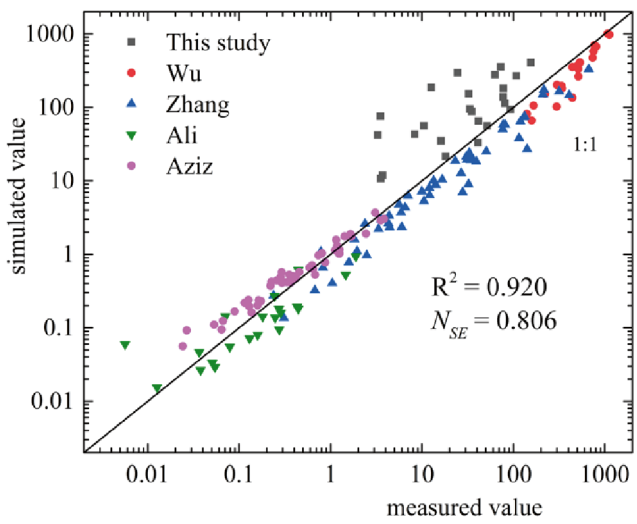

(b). The comparision of simulated and measured values in formula (17)

Fig. 6 Relationships between Φ and θ and the fitting precision of formula (17). (**a**) The relationship between Φ and θ. (**b**) The comparison of simulated and measured values in formula (17)

port capacity Φ was shown in Fig. 7a. It showed that the sediment transport capacity Φ increased in terms of its power function with an increasing stream power ($R^2 = 0.9458$). The relation can be expressed by formula (18):

$$\Phi = 0.0209W^{*1.3067}R^2 = 0.9458 \quad (18)$$

where W^* is the dimensionless stream power. Then, formula (18) was validated by the second set of data, as shown in Fig. 7b. The fitting precision R^2 was 0.970 and the N_{SE} value was 0.721. It can be seen from Fig. 7a that Aziz and Scott (1989) obtained a smaller sediment transport capacity under the same stream power, meaning that this formula is not well applicable

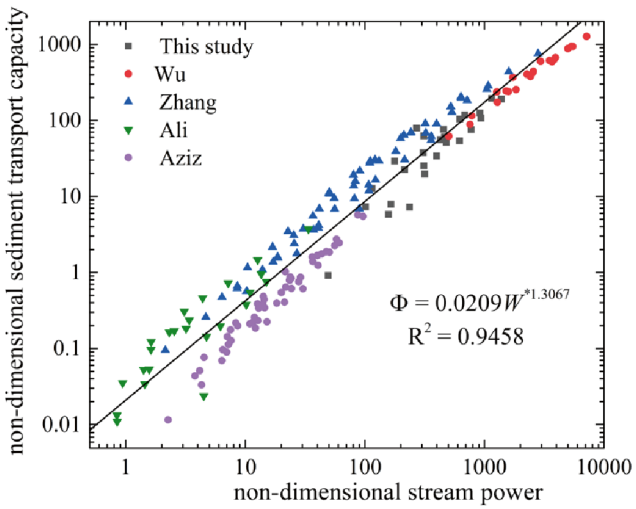

(a). The relationship between Φ and W^*

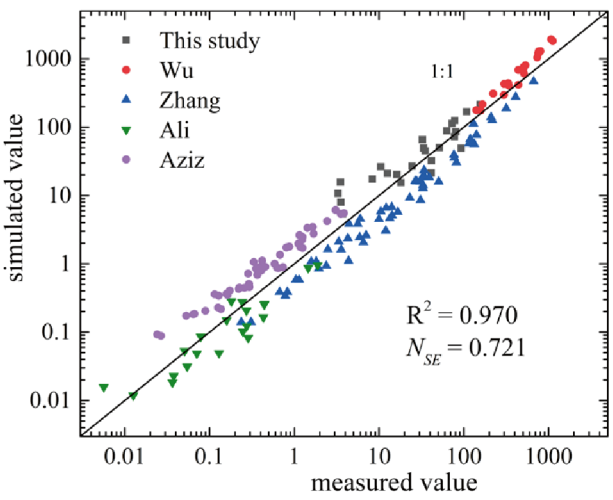

(b). The comparision of simulated and measured values in formula (18)

Fig. 7 Relationships between Φ and W^* and the fitting precision of formula (18). (**a**) The relationship between Φ and W^*. (**b**) The comparison of simulated and measured values in formula (18)

to the calculation in Aziz and Scott (1989). The reason is that Aziz and Scott (1989) carried out their experiments using a flume covered with soils under gentle slopes (3 ~ 10%) and large flow discharges. Therefore, the measured sediment transport capacity here is an unsaturated value.

(4) The response relationship between dimensionless unit stream power P^* and dimensionless sediment transport capacity Φ was shown in Fig. 8a . It showed that the sediment transport capacity Φ increased in terms of its power function with an increasing unit stream power (R^2=0.8847). The relation can be expressed by formula (19):

$$\Phi = 1.8927P^{*1.1961}R^2 = 0.8847 \quad (19)$$

where P^* is the dimensionless unit stream power. Then, formula (19) was validated by the second set of data, as shown in Fig. 8b. The fitting precision R^2 was 0.898 and the N_{SE} value was 0.495.

(5) The response relationship between dimensionless effective stream power $W_{eff}{}^*$ and dimensionless sediment transport capacity Φ was shown in Fig. 9a. It showed that the sediment transport capacity Φ increased in terms of its power function with an increasing effective stream power (R^2 = 0.9692). The relation can be expressed by formula (20):

$$\Phi = 0.0036W_{eff}{}^{*1.0927}R^2 = 0.969 \quad (20)$$

where $W_{eff}{}^*$ is the dimensionless effective stream power. Then, formula (20) was validated by the second set of data, as shown in Fig. 9b. The fitting precision R^2 was 0.975, and the N_{SE} value was 0.797. The simulated and measured values are around the 1:1 line, indicating that the effective stream power can better predict the sediment transport capacity.

The dimensionless effective stream power $W_{eff}{}^*$ appeared later than other parameters, which was proposed by Govers (1992) based on the concept of flow shear stress. It mainly refers to the residual net output power of water flow without losses due to the shear stress. Thus, the value of the effective stream power can also reflect sediment transport capacity. The larger the effective stream power is, the greater would be the output energy of the water flow. The flow with high energy can transport more sediments; this is why the effective stream power is significantly correlated with the sediment transport capacity.

Actually in the real world, both flow velocity and shear stress are easier to obtain through the measured water depth. Both cohesive and cohesionless soils can be transported by water flow under natural conditions. However, their transport processes differ owing to mutual adhesion between the particles; the sediment incipience of cohesive soil particles is in blocks when eroded by currents, while the cohesionless soil particles are transported from one to the next. To avoid the impact of transient transport characteristics of different soil types on sediment transport, the energy parameter would

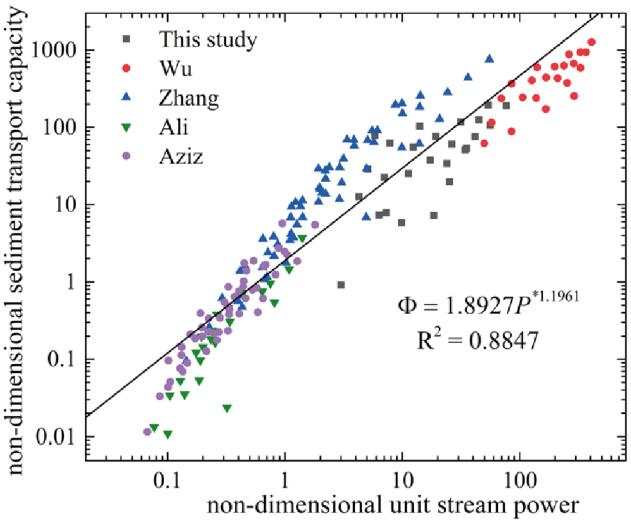

(a). The relationship between Φ and P*

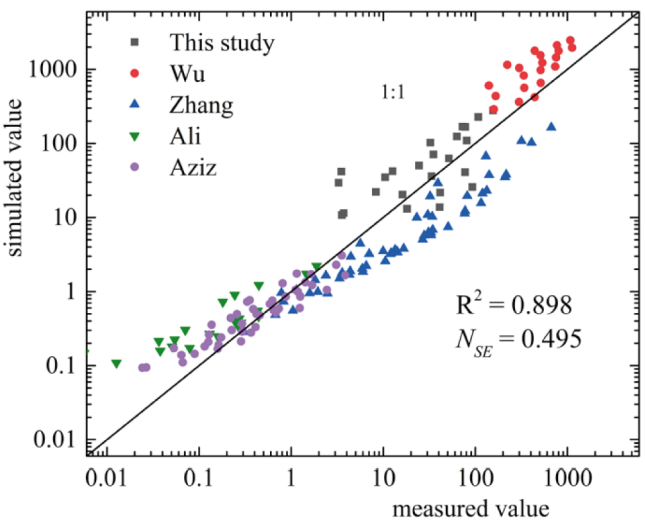

(b). The comparision of simulated and measured values in formula (19)

Fig. 8 Relationships between Φ and *P** and the fitting precision of formula (19). (**a**) The relationship between Φ and *P**. (**b**) The comparison of simulated and measured values in formula (19)

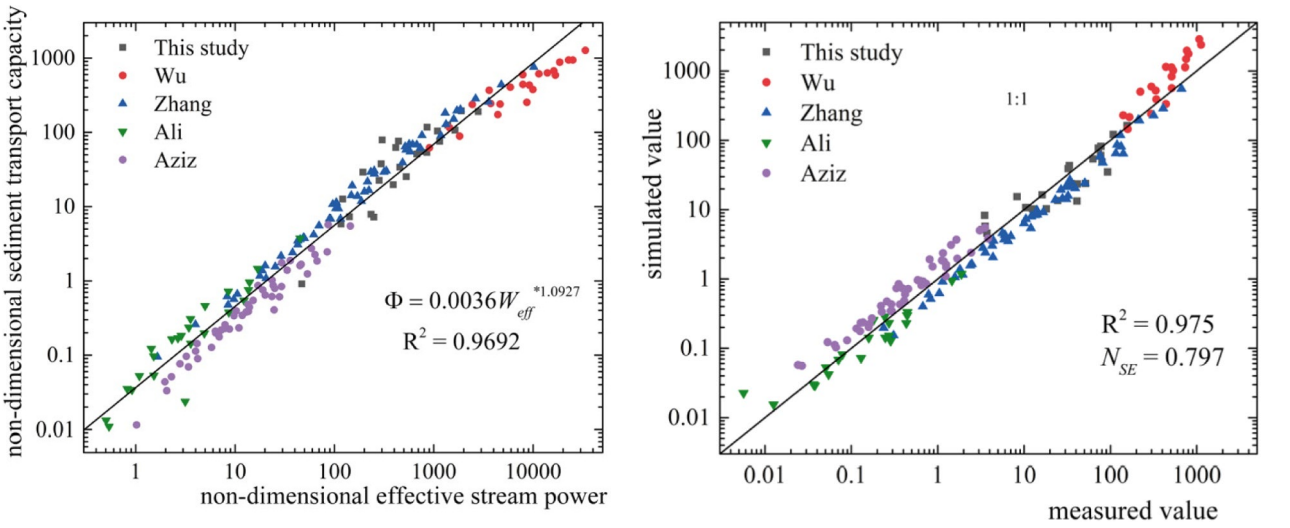

(a). The function relationship betwee Φ and W_{eff}^{*}

(b). The comparision of simulated and measured values in formula (20)

Fig. 9 Relationships between Φ and *W*eff* and the fitting precision of formula (20). (**a**) The function relationship between Φ and *W*eff*. (**b**) The comparison of simulated and measured values in formula (20)

be more appropriate than flow velocity or shear stress. The energy parameters can also reflect the energy consumption for the entire process of sediment transportation. The stream power and effective stream power all can be seen as appropriate energy parameters, but after analyzing the response relationship between flow intensity parameters and sediment transport capacity, this study employed the effective stream power to derive a formula for sediment transport capacity because of the higher R^2 (0.969) and N_{SE} (0.797).

3.2 Empirical formula for sediment transport capacity

The relationship between the dimensionless sediment transport capacity and dimensionless effective stream power can also be expressed by formula (21):

$$\Phi = \mathrm{K} W_{eff}^{*b} \tag{21}$$

Sediment transport coefficient K is a comprehensive coefficient representing the overall state of water flows and soils (Zhao et al. 2020). It is sensitive to multiple factors such as the equilibrium condition, saturation, and sediment characteristics. In this study, the dimensionless theory has eliminated the influence of median particle size. Therefore, K would only be influenced by the equilibrium condition and saturation. The volumetric sediment concentration S_v indicates the percentage of sediments in water flows per unit volume. It could depict the saturated state of sediments. The relationship between volumetric sediment concentration S_v and sediment transport coefficient K is analyzed as shown in Fig. 10.

It showed that sediment transport coefficient K exhibited an increasing trend as the volumetric sediment concentration S_v increased. According to SPSS correlation analysis, the Pearson index between sediment transport coefficient K and volumetric sediment concentration is 0.393. These two parameters are negatively correlated and their relationship can be expressed as follows:

$$K = 0.0576 S_v^{0.1551} R^2 = 0.393 \tag{22}$$

Then, the dimensionless sediment transport capacity Φ can be seen as a dependent variable. It would be

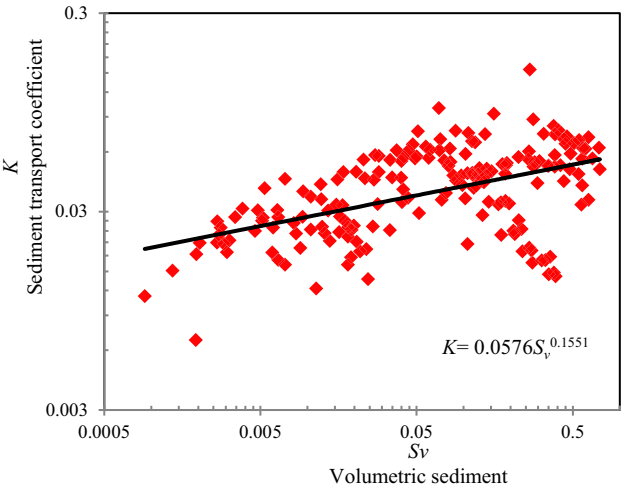

Fig. 10 Relationships between K and Sv

$$\Phi = 0.1742 S_v^{0.322} {W_{\text{eff}}}^{*0.949} R^2 = 0.989 \quad (23)$$

The proposed formula considered the volumetric sediment concentration, indicating whether the sediment is saturated or not. The dimensionless effective stream power was correlated with mean velocity, water depth, slope gradient, sediment particle density, and gravitational constant. Therefore, the proposed formula showed high fitting accuracy and can predict the sediment transport capacity effectively. However, in formula (23), both volumetric sediment concentration S_v and dimensionless sediment transport capacity are unknown parameters; hence, it needs to be further deduced by the implicit function method.

As sediment transport capacity can also be expressed by

$$T_c = S_v \gamma_s q \quad (24)$$

By introducing formula (23) into the formula (24) for calculating dimensionless sediment transport capacity in Table 4, it can be obtained that

$$= \frac{S_v \gamma_s q}{\gamma_s \sqrt{\left(\frac{\gamma_s}{\gamma} - 1\right) g d_{50}^3}} \quad (25)$$

When considering the formula (25) is equal to formula (23), it can be concluded that

$$\frac{S_v \gamma_s q}{\gamma_s \sqrt{\left(\frac{\gamma_s}{\gamma} - 1\right) g d_{50}^3}} = 0.1742 S_v^{0.322} {W_{\text{eff}}}^{*0.949} \quad (26)$$

The volume soil concentration can be calculated as

$$S_v^{0.678} = \frac{0.1742 {W_{\text{eff}}}^{*0.949} \sqrt{\left(\frac{\gamma_s}{\gamma} - 1\right) g d_{50}^3}}{q} \quad (27)$$

If the parameter related to soil types (d_{50}, γ_s) and runoff conditions (W_{eff}^*, q) can be obtained, the volume soil concentration S_v can be determined. Then a formula for dimensionless sediment transport capacity is derived by integrating formula (24) and formula (27):

$$T_c = S_v \gamma_s q = \frac{0.076 {W_{\text{eff}}}^{*1.4} \gamma_s g^{0.7374} d_{50}^{2.2125} (\gamma_s - \gamma)^{0.7374}}{q^{0.475} \gamma^{0.7374}} \quad (28)$$

By substituting $\gamma = 1$, $g = 9.8$ in formula (28), it would be

$$T_c 0.41 [\gamma_s (\gamma_s - 1)^{0.74} d_{50}^{2.21}] \frac{W_{eff}^{*1.4}}{q^{0.48}} \quad R^2 = 0.989 \quad (29)$$

$$X = \gamma_s (\gamma_s - 1)^{0.74} d_{50}^{2.21} \quad (30)$$

The formula (29) can be used to calculate the sediment transport capacity. When the soil types and flow conditions are determined, the X is a constant and sediment transport capacity would be mainly affected by the effective stream power and unit discharges. This formula is simple in form and has a high fitting degree. In addition, this formula considers the relationship between volumetric sediment concentration and sediment transport capacity. In the case of both parameters are unknown, an implicit function mathematical method was used for deriving a simplified calculation formula. As this formula considered the effective stream power as an important parameter, it can be applied to both cohesive and cohesionless soils, which will provide better results for predicting the sediment transport capacity.

To evaluate the applicability of formula (29), Fig. 11 shows the relationship between the measured value and calculated value of sediment transport capacity.

It can be seen in Fig. 11 that the calculated and measured value are around the 1:1 line ($R^2 = 0.985$, $N_{\text{SE}} = 0.884$), although this study included a series of data from this experiment, Wu's silty test, Zhang's, and Ali's and Aziz's cohesionless soil tests (Wu et al. 2016; Zhang et al. 2011; Ali et al. 2012; Aziz and Scott 1989). It means that this formula is applicable to calculate the sediment transport capacity of cohesive and cohesionless soil particles.

4 Discussion

4.1 Relationship between T_c, S, and q

Energy slopes and unit discharge are two main factors affecting the sediment transport capacity. This paper studied the

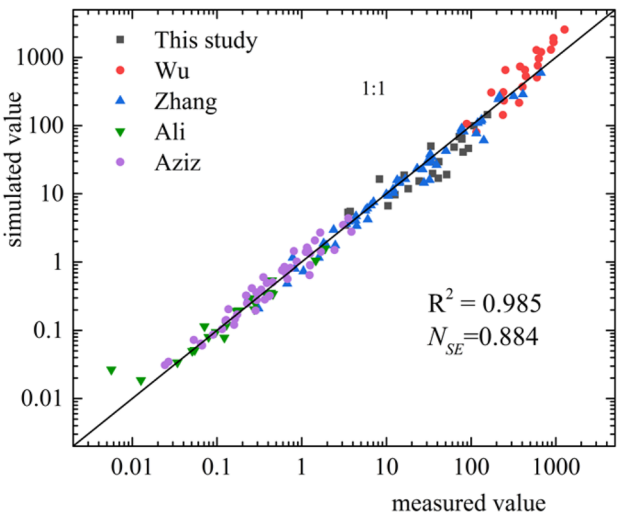

Fig. 11 Comparison between simulated and measured value of formula (29)

three-dimensional relationship between slope, unit discharge, and sediment transport capacity under 92 sets of tests with two different loess soils. It was concluded that there was a power function relationship between energy slopes, unit discharge, and sediment transport capacity:

$$T_c = 33496.5S^{1.086}q^{1.372}R^2 = 0.984N_{\mathrm{SE}=0.959} \quad (31)$$

The exponents were different in Zhang et al. (2009), Wu et al. (2016), and Mahmoodabadi et al. (2014a), as shown in Table 6 owing to different slopes, discharges, and especially the median particle size. For example, Zhang et al. (2009) selected fine sand, and their energy slope ranged from 8.8 to 46.6%, which was steeper than that used in this study. Mahmoodabadi et al. (2014a) used fine sand with energy slope ranging between 2 and 6%. This study and Wu et al. (2016) conducted experiments using soil samples with a larger median particle size than that in the other two studies.

Then, the energy slope and unit discharges in this experiment were substituted into these formulas in Table 6 to evaluate their applicability. The comparison between the simulated value and measured sediment transport capacity is shown in Fig. 12a.

It can be seen from Fig. 12 that most results obtained by formula (16) were scattered around 1:1 line except for some simulated values with a low sediment transport capacity ($R^2 = 0.984$). However, the simulated values through Zhang's formula (Zhang et al. 2009) were lightly larger than the measured values, which showed a relatively general applicability ($R^2 = 0.892$). The calculated values using Wu's formula were significantly larger than measured ones ($R^2 = 0.653$), which may have something to do with the steep slopes Wu et al. (2016) chose. The distribution of calculated points obtained by Mahmoodabadi's formula was rather dispersed ($R^2 = 0.704$), and this may because Mahmoodabadi et al. (2014a) considered a wide range of median particle sizes.

4.2 Comparison of prediction models

The formulas of sediment transport capacity obtained in this study are compared with Eqs. (1), (3), (4), and (5) as follows. Equation (4) depicts the relationship between sediment transport capacity T_c, median particle size d_{50}, slope gradients S, and flow discharges Q. As the flow discharge is sensitive to the width of test flumes, it should be converted into the unit discharge q. In this way, Eq. (4) can be expressed as

$$T_c = 0.17 \times 10^6 \frac{(0.2q)^{1.46}}{d_{50}^{0.5}} S^{2.89} \quad (32)$$

It also can be concluded that

$$T_c = 16216 \frac{q^{1.46}}{d_{50}^{0.5}} S^{2.89} \quad (33)$$

According to Eqs. (1), (3), (31), and (5), the relationship between measured and simulated values of sediment transport capacity was established as follows: It can be seen that in the left half of the Fig. 13a, the simulated values obtained by the ANSWERS model (Areal Nonpoint Source Watershed Environment Response Simulation) (Beasley et al. 1980) and the measured values showed zonal distribution and were relatively scattered on both sides of the 1:1 line. This might be because this model only considered the unit discharge as a single factor affecting sediment transport capacity. The fitting degree R^2 equals to 0.854, and N_{SE} equals to 0.796, indicating that the ANSWERS model can predict a relatively accurate T_c. However when predicting the sediment transport capacity of different soil types, the ANSWERS model is not the best choice. Figure 13 b shows that the simulated values using the improved WEEP model (Zhang et al. 2008) were mostly larger than the measured data. The fitting accuracy $R^2 = 0.67$ and $N_{\mathrm{SE}} = 0.188$. This might be because the improved WEPP model was established when considering only one sediment particle size ($d_{50} = 0.28$ mm), which cannot reflect the influence of the varied median sediment particle size on the sediment transport capacity. Therefore, there was an evident deviation when predicting the sediment transport capacity of flows with other median particle sizes. Further, Fig. 13c illustrates that the Zhang's formula (Zhang et al. 2011) with fitting degree $R^2 = 0.464$ and $N_{\mathrm{SE}} = 0.017$. Its simulated values are larger than measured ones, and their deviations maybe due to different types of soils. In this study, both Wu et al. (2016) and Aziz and Scott (1989) selected loess containing cohesive particles, and they obtained the most prominent deviations between measured and simulated values. Zhang et al (2011), Aziz and Scott (1989), and Ail et al. (2012) conducted experiments on cohesionless sand, and the deviation between

Table 6 The applicability of various models

Model	Slope/%	Unit discharge/$m^2\ s^{-1}$	Median particle size/mm	Formulas
This study	7 ~ 21.3	0.00014 ~ 0.00526	0.04 ~ 0.095	$T_c = 33496.5S^{1.086}q^{1.372}$
Zhang	8.8 ~ 46.6	0.000625 ~ 0.005	0.28	$T_c - 19831S^{1.227}q^{1.237}$
Wu	10.51 ~ 38.39	0.00111 ~ 0.00378	0.04	$T_c = 224S^{0.914}q^{1.297}$
Mahmoodabadi	2 ~ 6	0.005972 ~ 0.0122	0.19 ~ 0.77	$T_c = 8590.1S^{1.972}q^{0.855}$

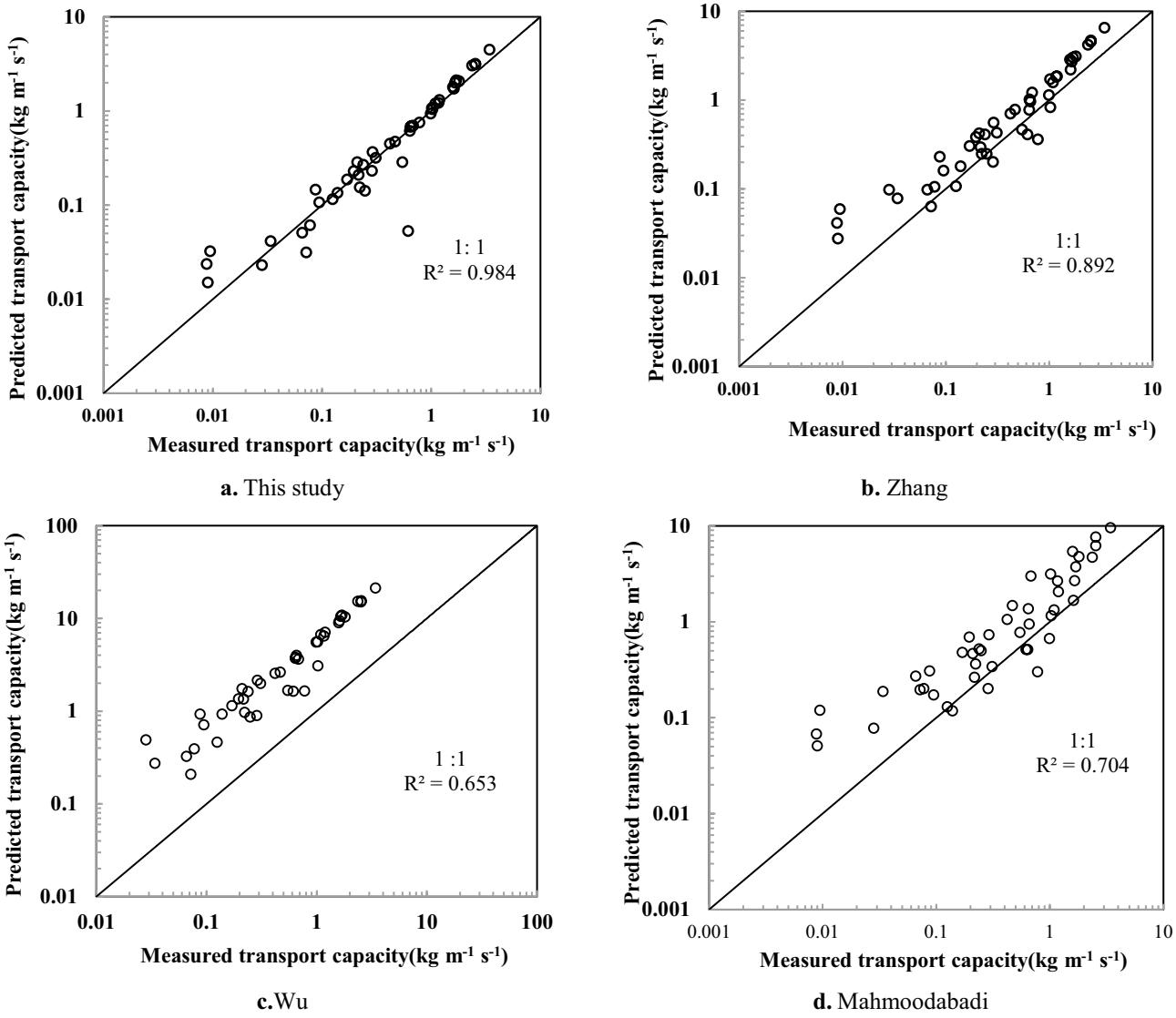

Fig. 12 Relationships between simulated and measured sediment transport capacity of Zhang, Wu, and Mahmoodabadi. (**a**) This study. (**b**) Zhang. (**c**)Wu. (**d**) Mahmoodabadi

measured and simulated values was insignificant. It indicates that Zhang's formula (Zhang et al. 2011) was more applicable for predicting the sediment transport capacity of cohesionless soils. It can be seen from Fig. 13d that the model proposed by Ali et al. (2012) yielded $R^2 = 0.797$ and $N_{SE} = 0.425$. When the sediment transport capacity is at a low or a high value, the deviation between measured and simulated values occurs. It indicates that the Ali's formula is more applicable to soil-laden flows with a transport capacity of 0.2 ~ 2 kg/(m s).

Based on the above comparison, it is concluded that each model has its advantages and limitations. The median particle size, hydraulic parameters, experimental condition, and soil characteristics all influence the prediction of sediment transport capacity. The dimensionless method is an effective method that can model the transport capacity considering compound parameters. However, to model sediment transport capacity for natural conditions, it is necessary to explore more direct factors affecting the sediment transport capacity in the process of water erosion in future research.

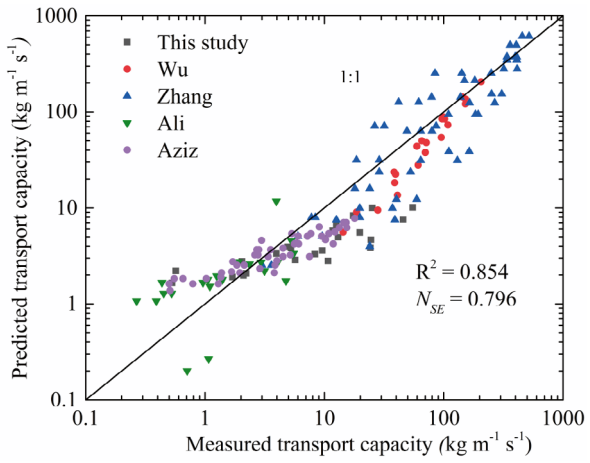

(a). The comparision between simulated values and measured values in ANSWERS model

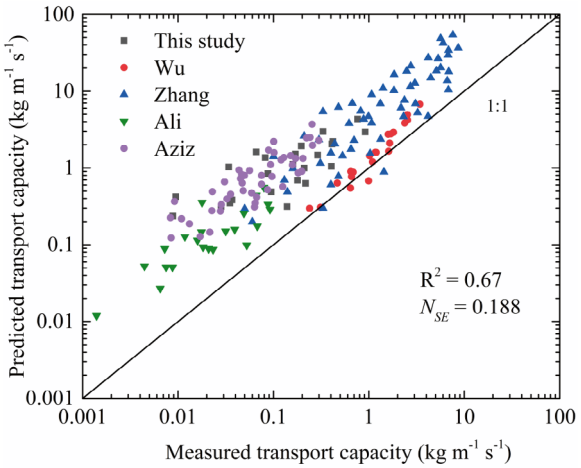

(b). The comparision between simulated values and measured values in improved WEPP model

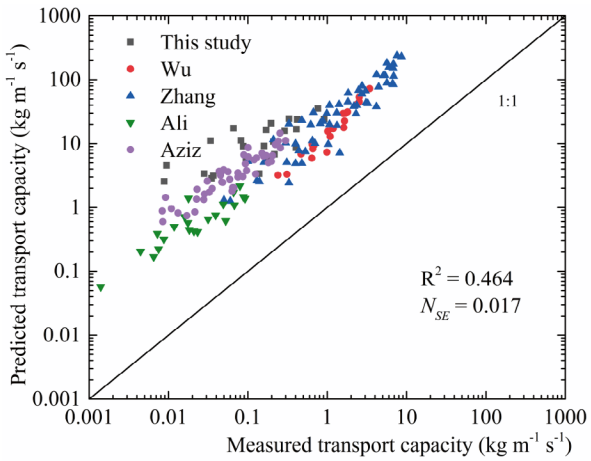

(c). The comparision between simulated values and measured values inZhang's model

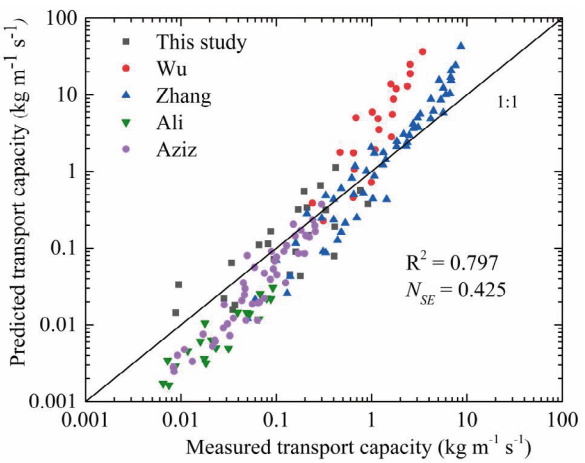

(d). The comparision between simulated values and measured values in Ali's model

Fig. 13 Comparison between simulated and measured value of four models. (**a**) The comparison between simulated values and measured values in ANSWERS model. (**b**) The comparison between simulated values and measured values in improved WEPP model. (**c**) The comparison between simulated values and measured values in Zhang's model. (**d**) The comparison between simulated values and measured values in Ali's model

5 Conclusions

This study selected sandy loess and loess soil with different median particle sizes to mainly investigate the response relationship between sediment transport capacity and flow intensity parameters. The aim of this study was to derive a formula for calculating sediment transport capacity applicable to cohesive and cohesionless soils. The main conclusions are as follows:

(1) For cohesionless soils, the shear stress was observed as an effective parameter in contrast to the flow velocity parameter. However, the shear stress cannot be used to calculate the sediment transport capacity of cohesive soils. Compared with the above single parameters, the compound parameter stream power especially the effective stream power was observed as the best predictor for sediment transport capacity.

(2) The influence of median particle sizes on the sediment transport capacity can be eliminated by making the parameters dimensionless. And then, the relationship between the sediment transport coefficient K and volumetric sediment concentration was analyzed theoretically to verify that the volumetric sediment concentration is an essential predictor.

(3) The proposed prediction model for sediment transport capacity was derived using the dimensional effective stream power and volumetric sediment concentration. It was observed that the proposed model had a wider applicability than the four existing models.

In conclusion, the proposed prediction model here provides a basis for predicting the sediment transport capacity of different soils types. However, as the sediment transport capacity is sensitive to numerous parameters, exploring direct influencing factors is necessary to accurately simulate natural conditions.

Acknowledgements Many thanks for the professional native speakers in editage who gave useful advice on scientific writing of this manuscript.

Author contribution Jingwen Wang: data curation, formal analysis, methodology, writing-original draft, writing-review and editing; Chenye Gao: conceptualization, funding acquisition, project administration, writing-original draft; Xile Liu: data curation; Guangming Tan: writing-review and editing;

Funding This research was supported financially by the Central Public-interest Scientific Institution Basal Research Fund (Grant No. Y120002) and POWERCHINA Chengdu Engineering Corporation Limited (Contract No. DJ-ZDXM-2020–42).

Data availability All data used during the study are available from the corresponding author.

Declarations

Conflicts of interest The authors declare no competing interests.

References

Abrahams AD, Li G, Parsons AJ (2015) Rill hydraulics on a semi-arid hillslope, southern Arizona. Earth Surf Process Landf 21(1):35–47

Ahmadi SH, Amin S, Keshavarzi AR, Mirzamostafa N (2006) Simulating watershed outlet sediment concentration using the answers model by applying two sediment transport capacity equations. Biosyst Eng 94(4):615–626

Ali M, Sterk G, Seeger M, Boersema M, Peters P (2012) Effect of hydraulic parameters on sediment transport capacity in overland flow over erodible beds. Hydrol Earth Syst Sci 16(2):591–601

Aziz NM, Scott DE (1989) Experiments on sediment transport in shallow flows in high gradient channels. Hydrolog Sci J 34(4):465–478

Bagnold RA (1966) An approach to the sediment transport problem from general physics. U.S. Geol Surv Prof Pap 422–I, 231–291.

Beasley DB, Huggins LF, Monke EJ (1980) ANSWERS: a model for watershed planning. T ASABE 23(4):938–0944

De Roo AP (1996) The LISEM project: An introduction. Hydrol Process 10(8):1021–1025

Dunkerley D (2010) Estimating the mean speed of laminar overland flow using dye injection-uncertainty on rough surfaces. Earth Surf Process Landf 26(4):363–374

Finkner SC, Hearing MA, Foster GR, Gilley JE (1989) A simplified equation for modeling sediment transport capacity. T ASABE 32(5):1545–1550

Govers G (1990) Empirical relationships for the transport capacity of overland flow. Iahs Publication 189.

Govers G (1992) Evaluation of transporting capacity formulae for overland flow. Overland Flow, Hydraulic and Erosion Mechanics. 243–273.

Govers G, Rauws G (2010) Transporting capacity of overland flow on plane and on irregular beds. Earth Surf Process Landf 11(5):515–524

Hao HX, Wang JG, Guo ZL, Hua L (2019) Water erosion processes and dynamic changes of sediment size distribution under the combined effects of rainfall and overland flow. CATENA 173:494–504

Huang C, Wells LK, Norton LD (1999) Sediment transport capacity and erosion processes: model concepts and reality. Earth Surf Process Landf 24(6):503–516

Li G, Abrahams AD (1999) Controls of sediment transport capacity in laminar interrill flow on stone — covered surfaces. Water Resour Res 35(1):305–310

Li P, Zhang KD, Wang JW, Feng DQ (2021) Response of interrill erosion to flow parameters of sand loess in regions with high and coarse sediment yields. J Hydrol 592:125786.

Li P, Zhang KD, Wang JW, Meng H (2020) Nondimensional sediment transport capacity of sand soils and its response to parameter in Loess Plateau of China. Hydrol Process 34(3):823–835

Liu JE, Wang ZL, Yang XM, Jiao N, Shen N, Ji PF (2014) The impact of natural polymer derivatives on sheet erosion on experimental loess hillslope. Soil till Res 139:23–27

Liu Y, Fu B, Lü Y, Wang Z, Gao G (2012) Hydrological responses and soil erosion potential of abandoned cropland in the Loess Plateau. China Geomorphology 138(1):404–414

Luan LL, Zhang GH, Wang LL, Han YF (2016) Study on sediment transport capacity of overland flow based on stream power. J Sediment Res 2:61–67 (**(in Chinese with English abstract)**)

Luk SH, Merz W (1992) Use of the salt tracing technique to determine the velocity of overland flow. Soil Tech 5(4):289–301

Mahmoodabadi M, Ghadiri H, Rose C, Yu B, Rafahi H, Rouhipour H (2014a) Evaluation of GUEST and WEPP with a new approach for the determination of sediment transport capacity. J Hydrol 513:413–421

Mahmoodabadi M, Ghadiri H, Yu B, Rose C (2014b) Morpho-dynamic quantification of flow-driven rill erosion parameters based on physical principles. J Hydrol 514:328–336

Merten GH, Nearing MA, Borges AL (2001) Effect of sediment load on soil detachment and deposition in rills. Soil Sci Sco Am J 65(3):861–868

Mu HL, Yu XJ, Fu SH, Yu BF, Liu YN, Zhang GH (2019) Effect of stem basal cover on the sediment transport capacity of overland flows. Geoderma 337:384–393

Nearing, MA, Forster GR, Lane LJ, Finkner SC (1989) A process-based soil erosion model for USDA-Water Erosion Prediction Project Technology. T ASABE 32(5): 1587¬1593.

Nearing MA, Norton LD, Bulgakov DA (1997) Hydraulics and erosion in eroding rills. Water Resour Res 33(4):865–876

Pieri L, Bittelli M, Hanuskova M, Ventura F, Vicari A, Pisa PR (2009) Characteristics of eroded sediments from soil under wheat and maize in the north italian apennines. Geoderma 154 (1–2): 0–29.

Prosser IP, Rustomji P (2000) Sediment transport capacity relations for overland flow. Prog Phys Geogr 24(2):179–193

Shang HX, Zhang KD, Wang ZH, Yang J, He MY, Pan XC, Fang CY(2020) Effect of varying wheatgrass density on resistance to overland flow. J Hydrol 591:125594.

Tian P, Zhai J, Zhao G, Mu X (2016) Dynamics of runoff and suspended sediment transport in a highly erodible catchment on the Chinese Loess Plateau. Land Degrad Dev 27(3):839–850

Wang C, Wang B, Wan Y, Wang Y, Zhang W, Zhang XJ (2020a). Rare earth elements tracing interrill erosion processes as affected by near-surface hydraulic gradients. Soil Till Res 202: 104673.

Wang C, Wang B, Wang Y, Zhang W, Yan Y (2020b) Impact of near-surface hydraulic gradient on the interrill erosion process. Eur J Soil Sci 71(4):598–614

Wang JW, Zhang KD, Li P, Meng Y, Zhao LY(2021) Hydrodynamic characteristics and evolution law of roll waves in overland flow. Catena 198:105068.

Wang JW, Zhang KD, Yang MY, Meng H (2019) Li P The effect of roughness and rainfall on hydrodynamic properties of overland flow. Hydro Res 50(5):1324–1343

Wang SY, Flanagan DC,Engel BA, Zhou N (2021) Prediction of rill sediment transport capacity under different subsurface hydrologic conditions. J Hydrol 598: 126410

Wu B, Wang Z, Shen N, Wang S (2016) Modelling sediment transport capacity of rill flow for loess sediments on steep slopes. CATENA 147:453–462

Wu B, Wang ZL, Zhang QW,Shen N, Liu J, Wang S (2018) Evaluation of shear stress and unit stream power to determine the sediment transport capacity of loess materials on different slopes.J Soils Sediments 18:116–127

Wu B, Li LD, Xu L, Wei XD, Li XL (2021) The influence of slopes on interrill erosion processes using loessial soil.J Soils Sediments. (online: https://doi.org/10.1007/s11368-021-03018-6)

Yalin MS (1963) An Expression for Bed-Load Transportation. J Hydraul Eng 89(3):221–250

Yu B, Zhang G, Fu X (2015) Transport capacity of overland flow with high sediment concentration. J Hydrol Eng 20(6):1–10

Zhang GH, Liu BY, Zhang XC (2008) Applicability of WEPP sediment transport equation to steep slopes. T ASABE 51(5):1675–1681

Zhang GH, Wang LL, Tang KM, Luo RT, Zhang XC (2011) Effects of sediment size on transport capacity of overland flow on steep slopes. Hydrolog Sci J 56(7):1289–1299

Zhang GH (2000) Summary study on runoff detachment processes based on hydraulics. J Soil Water Conserv 14(3):112–115 ((**in Chinese with English abstract**))

Zhang GH, Liu YM, Han YF, Zhang XC (2009) Sediment transport and soil detachment on steep slopes: I. Transport capacity estimation. Soil Sci Soc Am J 73 (4): 1291–1297.

Zhang RB, Zhang LP, Fu XT (2017) Research on relationships between sediment yield and hydraulics parameters on slope. J Soil Water Conserv 31(5):81–86 ((**in Chinese with English abstract**))

Zhao G, Mu X, Wen Z, Wang F, Gao P (2013a) Soil erosion, conservation, and eco-environment changes in the Loess Plateau of China. Land Degrad Dev 24(5):499–510

Zhao GJ, Mu XM, Tian P, Wang F, Gao P (2013b) Climate changes and their impacts on water resources in semiarid regions: a case study of the Wei River basin. China Hydrol Process 27(26):3852–3863

Zhao LY, Zhang KD, Wu SF, Feng DQ, Wang JW (2020) Comparative study on different sediment transport capacity based on dimensionless flow intensity index. J Soil Sediment 20(4):1–17